Chapter 2

Synthesis and Characterization Techniques

Chapter 2

Synthesis and Characterization Techniques

2.1 Overview

This chapter provides a brief description of the various research techniques used for material synthesis, characterization, electrode fabrication and electrochemical measurements to develop potentially active OER electrocatalysts. To characterize the catalyst material used in the proposed studies, a variety of characterization techniques were employed, including X-ray diffraction pattern (XRD), fourier transform infrared spectroscopy (FT-IR), field emission scanning electron microscopy (FE-SEM) with energy dispersive X-ray analysis (EDAX or EDX), transmission electron microscopy (TEM) with high resolution micrograph analysis along with selected area electron diffraction (SAED) pattern studies, X-ray photoelectron spectroscopy (XPS), inductively coupled plasma-mass spectrometry (ICP-MS), and electrochemical measurements with cyclic voltammetry (CV), linear sweep voltammetry (LSV), electrochemical impedance spectroscopy (EIS), and chronoamperometry (CA).

2.2 Material synthesis techniques

The synthesis of high-quality powder samples is crucial for obtaining excellent quality single crystals and desired physical properties. To achieve this, several factors need to be considered, which are as follows.

- **Selection of appropriate synthesis route:** The synthesis method chosen depends on the desired material and its properties. Common methods include solid-state reactions, solution combustion, sol-gel, co-precipitation, hydrothermal synthesis and more. Each method has its own advantages and limitations, so careful consideration is necessary.

- **Purity of starting precursors:** The starting materials used should be of high purity to ensure the final product's quality. Impurities, even in small amounts, can significantly affect the crystal structure and physical properties.
- **Stoichiometric ratios**: To achieve the desired composition, it is essential to maintain the precise stoichiometric ratios of the constituent components. Achieving homogeneity and uniform distribution of elements in the powder mixture can be facilitated by using appropriate weighing and mixing processes, such as mechanical mixing or ball milling.
- **Reaction condition optimization:** The desired phase formation and crystal quality can only be attained by optimizing the reaction parameters, such as temperature, pressure, and reaction time.

In the present work, we have synthesized the samples via solid-state reaction route and solution combustion synthesis technique, which are described as follows.

2.2.1 Solid-state reaction or ceramic method

The solid-state reaction method is a widely used technique for the synthesis of polycrystalline solids from basic solid starting materials. It requires mechanical mixing of oxide powders, carbonates, followed by heat treatment. Generally, solids do not react at room temperature over an ordinary time scale. So, it is necessary to heat them at a much higher temperature. Factors that influence the solid-state reaction rate are structural properties of solids, reaction conditions, surface area, temperature, pressure, thermodynamic free energy change associated with the reaction [1, 2]. The advantages associated with this method are given below:

- Minimal production of byproducts
- Solvents is not required in the reaction.
- Structure purity along with desired properties.
- Large scale production.

- Environment-friendly.
- Simplicity and low cost.

The schematic block diagram, shown in **Figure 2.1**, displays a detailed procedure of the solid-state reaction method.

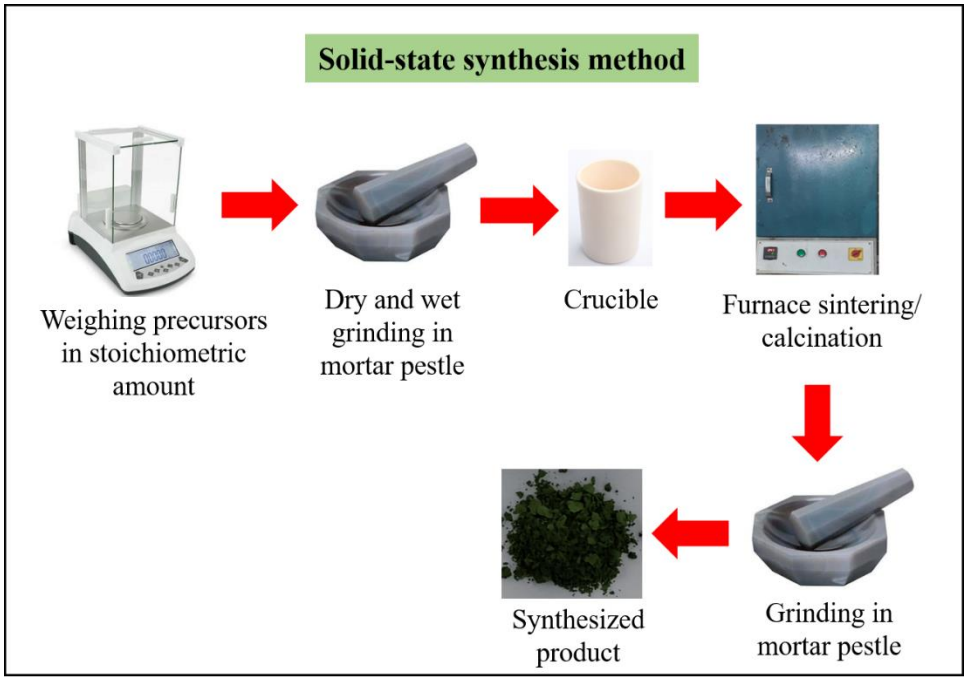

Figure 2.1 Schematic block diagram of solid-state synthesis procedure.

2.2.2 Solution combustion synthesis method

Solution combustion synthesis (SCS) is a quick, easy, efficient, and adaptable technique that is gaining a lot of attention worldwide for the preparation of oxide materials with controlled properties (high purity and homogeneity) for a variety of applications, including electronics, solid fuel cells, and electrocatalysis [3-6]. Although SCS is based on propellant and sol-gel chemistry, it can produce higher-quality final products more quickly than sol-gel [7]. There are three primary processes in solution combustion synthesis: i) production of the combustion mixture; ii) formation of the gel; and iii) burning of the gel. Simply said, SCS is the result of a

self-sustaining redox reaction between a fuel and an oxidant (often metal nitrates) in the presence of metal cations, which is started by a thermal or electrical energy source.

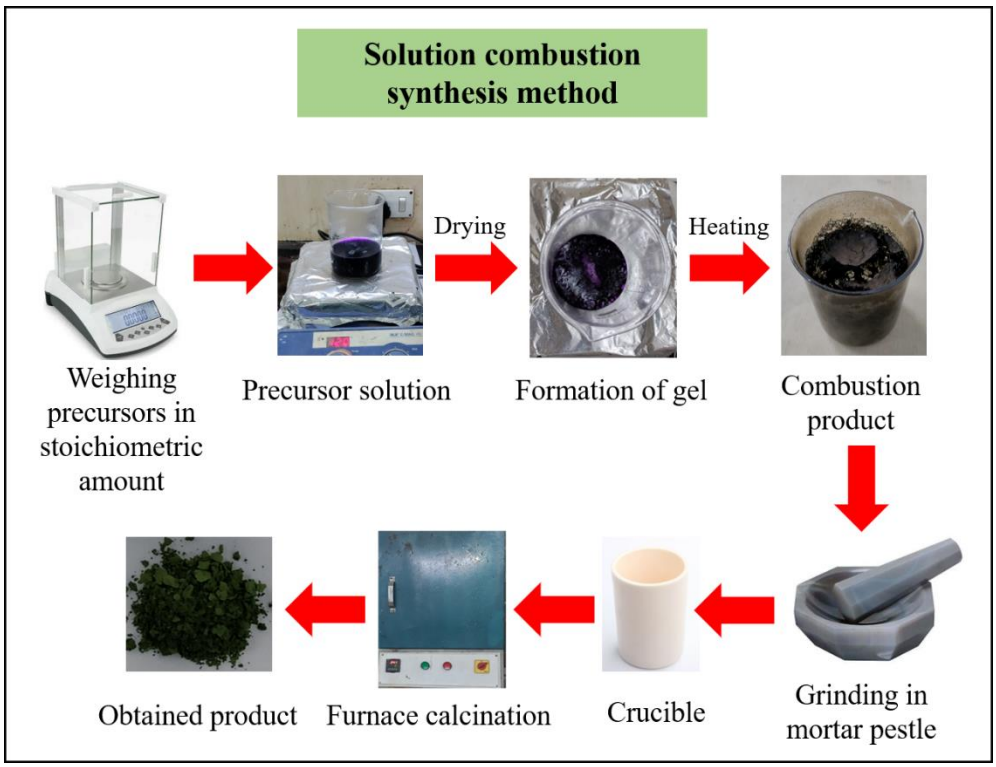

Figure 2.2 Schematic block diagram of solution combustion synthesis procedure.

Typically, the fuel is made up of organic materials (such as glycine, urea, citric acid etc.) that contain carbon, hydrogen, and nitrogen, which helps to release heat during combustion by forming CO_2, NO_2, and H_2O [8]. Patil et al. firstly reported the SCS of oxides by combining aluminum nitrate nonahydrate ($Al(NO_3)_3 \cdot 9H_2O$), the oxidant and urea ($CO(NH_2)_2$), the fuel, based on a stoichiometric balance of the redox mixture to attain aluminum oxide [9]. This process requires a moderate temperature to start the combustion reaction, which in turn creates a potent exothermic redox reaction that provides sufficient energy to build the metal oxide lattices. A high temperature is not necessary for this reaction to occur. This enables the solution precursors to be transformed into oxides at low process temperatures. The final properties of the resultant oxides that are produced from the SCS are highly dependent on the synthesis

parameters, such as, the fuel type, the metal cations precursors, the pH, the reducer to oxidizer ratio (ϕ), the atmosphere environment and initiation type [8, 9]. A detailed procedure of solution combustion synthesis method is shown in the schematic block diagram of **Figure 2.2**.

2.3 Material characterization techniques

The characterization techniques used in this study are described in the following section, which provides a brief overview of fundamentals of each method.

2.3.1 Powder X-ray diffraction (XRD)

The most common tool for phase confirmation of polycrystalline materials is powder X-ray diffraction (XRD), which produces a characteristic diffraction pattern fingerprint that are widely used for phase confirmation and/or identification. It is one of the most versatile methodologies, suitable for bulk materials (solid-solution) as well as for thin films to study the crystal structure, phase, and other structural parameters, such as average grain size, strain, crystallinity, and crystal defects [10]. Powder X-ray diffraction (XRD) is a non-destructive type of analytical technique based on constructive interference of monochromatic X-rays and a crystalline sample. It provides valuable insight about the lattice structure of a crystalline substance like unit cell dimensions, bond angles, chemical composition, and crystallographic structure of natural and manufactured materials [11]. In this technique, the diffraction pattern is measured using X-rays, with their wavelength (λ) falling within the same range (1-100 Å) as the inter-planer spacing (d) between the planes in the crystal system. The X-ray diffractometer consists of three basic components: (a) X-ray tube, (b) a sample holder, and (c) X-ray detector. The X-ray are generated by cathode ray tube (CRT), filtered to produce monochromatic radiation, collimated to concentrate, and directed towards the sample. The interaction of the incident monochromatic rays with the sample produces constructive interference (and diffracted ray) when condition satisfy Bragg's Law [12].

$$n\lambda = 2d\sin\theta \quad (2.1)$$

This equation relates the wavelength (λ) of electro-magnetic radiation to the diffraction angle (θ) and the lattice spacing (d) in a crystalline sample by scanning the sample through arrangement of 2θ angles. All the possible diffraction directions of the lattice are attained due to the random orientation of the powdered materials. **Figure 2.3** illustrates the Bragg's diffraction law [13]. The diffraction peaks depend upon the symmetry of the material's structure.

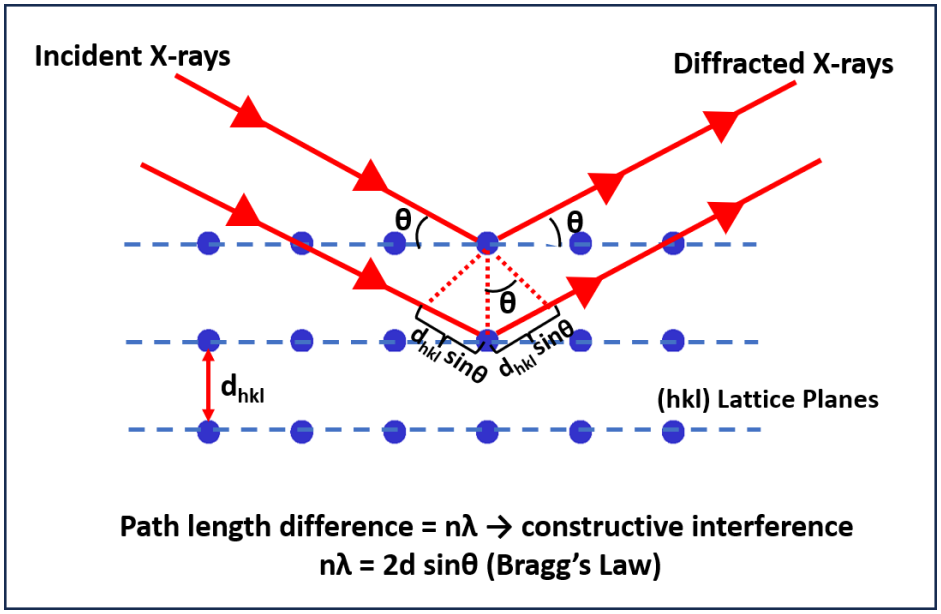

Figure 2.3 Schematic diagram of Bragg's diffraction law (adapted from [13]).

In this study, the X-ray patterns of all the samples were recorded on Rigaku Miniflex X-ray diffractometer using Ni-filtered Cu Kα radiation (λ = 1.54 Å) and applied voltage of 40kV in the 2θ range of 10–80º and a step size of 0.02º. The X-ray diffractometer used in our investigation is shown in **Figure 2.4**.

The powder XRD patterns were refined using FullProf Suite software in a Rietveld method. Based on a methodology developed by Hugo Rietveld in the 1960s, Xpert High Score (PANanylytical) is a commonly used refinement method for powder X-ray diffraction (XRD)

[14]. Using the Rietveld method, an estimated profile with all the instrumental and structural characteristics is fitted to the experimental data. The method utilizes the non-linear least-squares technique and demands an accurate approximation of numerous free parameters in the preliminary phase, such as unit cell dimensions, peak shape, and every single atomic coordinate in the crystal structure. With reasonable guesswork, other parameters can also be refined. In this manner, it is possible to refine the crystal structure of powder material using PXRD data. The successful outcome of the refinement method is directly correlated to the data quality of the model (includes initial approximation) and the user's experience.

Figure 2.4 Experimental setup of X-ray diffractometer, CIF-IIT (BHU), (Rigaku Miniflex II, Japan).

2.3.2 Scanning electron microscopy (SEM)

Electron microscopy is a pioneering imaging technique that is extensively employed in the scientific and technical communities to study the morphology and structure of nanomaterials. Scanning electron microscope is a type of electron microscope that creates image of the sample

by scanning it with high-energy electron beam, which collides with a sample's surface, causing a range of interactions that provide the information about the morphology and chemical composition of the sample. SEM can create extremely high-resolution images of a sample surface, displaying details with a size range of less than 1 to 5 nm. SEM micrographs feature a significant depth of field and a distinctive three-dimensional gaze that is helpful for analyzing the surface structure of a sample because of the extremely narrow electron beam [15, 16].

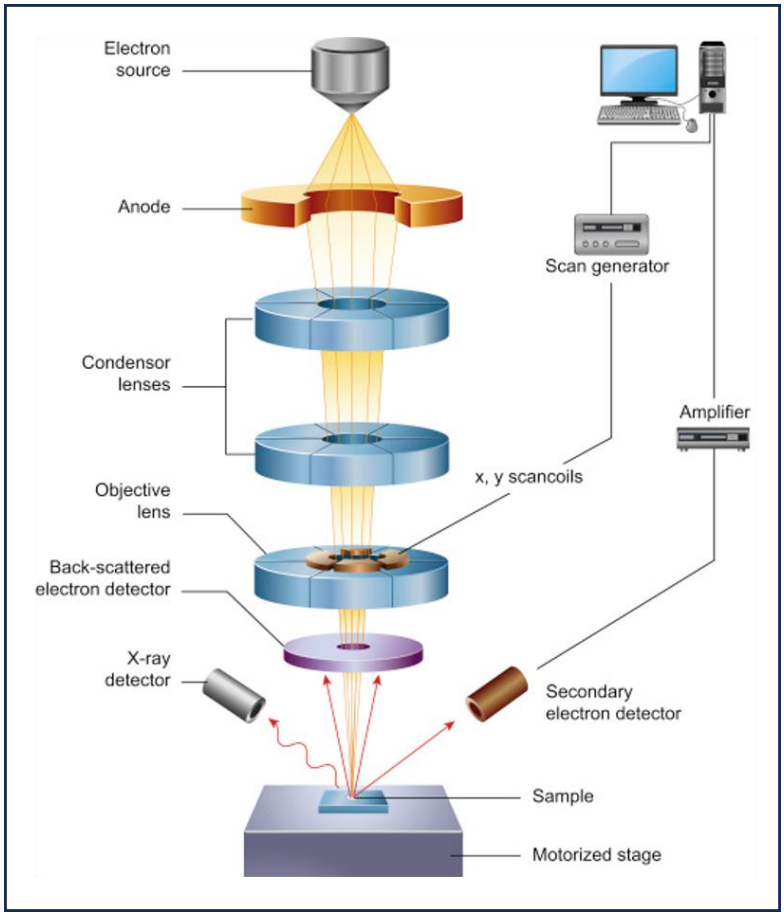

Figure 2.5 Schematic diagram of the core components of an SEM [17].

The standard configuration of high resolution-scanning electron microscopy (HR-SEM) is depicted in **Figure 2.5**. It comprises an electron source that generates and accelerates electrons through an accelerating anode, electromagnetic lenses that focus the electrons, a vacuum chamber, and a detector that gathers signals emitted from materials. High-energy electrons and

the specimen interact to cause scattering, which produces a variety of signals including auger electrons, backscattered electrons, secondary electrons, and distinctive X-rays. The sample's surface produces the auger electrons in a low-atomic-number molecule. The backscattered electrons are generated by elastic scattering and have high energy, while the inelastic scattering generates the secondary electrons having an energy of a few KeV. The secondary electron provides better spatial resolution for the imaging process [17]. Working distance, probe current, accelerating voltage, and astigmatism can all have an impact on the depth of field and resolution, which determine the quality of the images in a scanning electron microscope. In the present study, Nova Nano SEM 450 scanning electron microscope (SEM) equipped with EDAX - Ametek detector was employed to understand the morphology and chemical composition of prepared samples. **Figure 2.6** displays the image of HR-SEM.

Figure 2.6 Experimental setup of SEM measurement, CIF-IIT (BHU), (Nova Nano SEM 450).

The next section examines the examination of X-ray radiation emitted from the specimen to study quantitative and qualitative elemental information from a specific location of the specimen using the characteristic X-rays created because of electron bombardment in the SEM experiment.

2.3.3 Energy dispersive X-ray spectroscopy (EDS or EDX)

An analytical method called energy dispersive X-ray analysis (EDAX), also known as energy dispersive X-ray spectroscopy (EDS or EDX), is used in conjunction with transmission or scanning electron microscopy (SEM) to ascertain a sample's chemical composition, elemental fraction, and mapping (homogeneity) analysis, among other things. A non-destructive technique called EDX is utilised to quickly calculate all constituent elements with $Z \geq 11$ [18].

2.3.4 Transmission electron microscopy (TEM)

The transmission electron microscope (TEM) is a high magnification, multipurpose tool for examining the structural and morphological properties of materials, e.g., shape, size, and constituent distribution etc. Users can employ TEM in a variety of ways, depending on their needs. Examples of these include HRTEM (high-resolution TEM), selected area electron diffraction, and additional units like elemental mapping and EDX (electron dispersive X-ray spectroscopy) [19]. A transmission electron microscope (TEM) is made up of electron gun, vacuum system, electromagnetic lenses, high-voltage generator, recorders, and related electronics. TEM produces high-resolution images at the atomic length scale by using electrons with a lower wavelength. An anode accelerates a well-focused electron beam that is obtained from the electron cannon assembly and electromagnetic condenser lenses. The anode is usually at a potential of 100 KeV relative to the cathode. The condenser aperture, which blocks uncollimated electrons, limits the beam. The specimen is struck by a collimated high energy electron beam (200 KeV and above), which is then scattered based on the material's thickness and electron transparency. Transmission occurs for a portion of the dispersed electron beam that is changing in phase and amplitude during scattering. An image is formed on a phosphor screen or charge-coupled device camera by the objective lens focusing part of the scattered electron beam that is changing in phase and amplitude during the scattering process. Objective

apertures can be changed to improve contrast and block high-angle diffracted electrons. Data collection took place in transmission mode, with sample geometry restricted to very thin (less than 100 nm) samples.

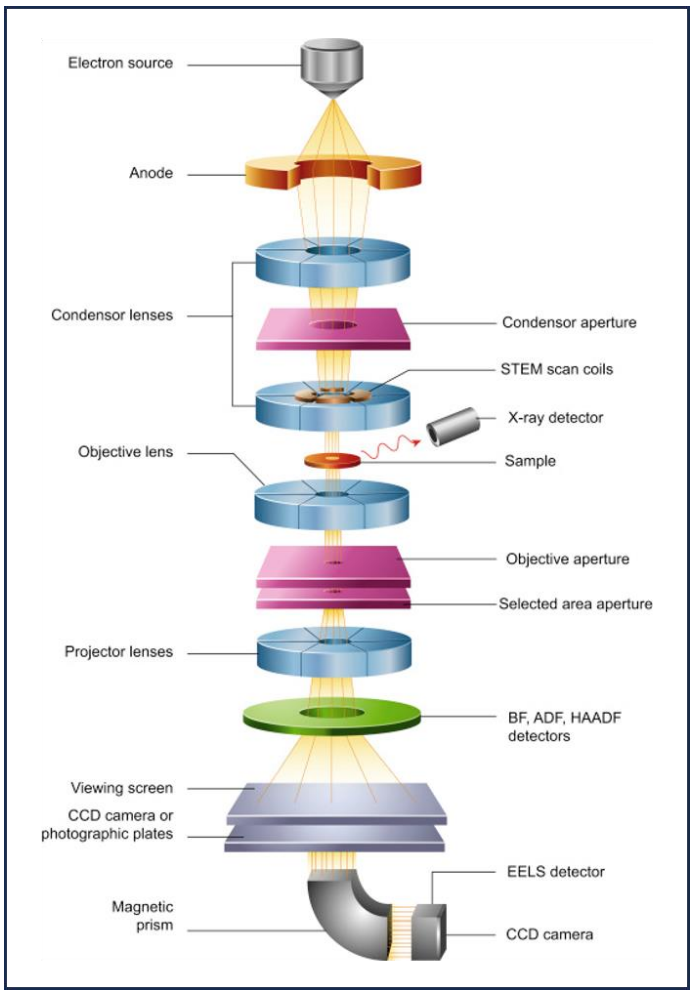

Figure 2.7 Schematic diagram of core components of a TEM [17].

Figure 2.7 illustrates a typical layout of high resolution- transmission electron microscope (HR-TEM) [17]. In this thesis, FEI Tecnai G2 20 TWIN-transmission electron microscope (USA) using a LaB_6 filament and an accelerating voltage of 200 kV, were employed to produce bright-field TEM micrographs and selected area diffraction patterns (SAED). Before placing a drop on a holey-carbon-coated copper grid (Pelco International, USA) for TEM imaging, samples were diffused in 20 millilitres of anhydrous ethanol and sonicated for 30 minutes.

Using Gatan Microscopy Suite (Digital Micrograph) and ImageJ software, HRTEM micrographs were captured and examined [20]. **Figure 2.8** shows the image of HR-TEM.

Figure 2.8 Experimental setup of TEM measurement, CIF-IIT (BHU), (FEI Tecnai G2 20 TWIN, USA).

2.3.5 X-ray photoelectron spectroscopy (XPS)

XPS is a non-destructive, surface-sensitive spectroscopic technique that assesses the chemical and electronic states of the constituent elements within a material, as well as the composition of those elements at the part per thousand level, using empirical formulas. It displays both the elements that are present and the elements to which they are bound. XPS is a high vacuum method that functions at about 10-6 Pa of vacuum. The present state of development is ambient pressure XPS, which can examine samples at pressures as high as many tens of millibars. The photoemission process serves as the foundation for this method. Using this technique, a high energy X-ray is directed towards the material surface. This causes the inner level electrons of the surface atom to absorb the photon energy (hυ), overcome their binding energy (E_B), and expel kinetic energy (E_{kin}) out of the surface within a range of 1-10 nm. The following Einstein equation describes this process:

$$E_{kin} = h\upsilon - E_B - W_f \tag{2.2}$$

After analyzing the energy spectrum of the photoelectrons released, an intensity spectrum as a function of binding energy is obtained. The element is characterised by the binding energy of each peak. Except for hydrogen and helium, all elements are readily detected by laboratory XPS. In addition to many other materials, XPS is frequently used to study semiconductors, metal alloys, inorganic compounds, catalysts, glues, polymers, ceramics, glasses, inks, woods, bones, teeth, medical implants, elements, biomaterials, viscous oils, and ion-modified materials [21]. The basic principle of XPS is shown in **Figure 2.9**. The XPS of the samples in the present work was performed using Thermo Fisher Scientific's K-Alpha spectrometer, which was equipped with an aluminium (Al Kα radiation) monochromator source running at 15 kV and 20 mA. **Figure 2.10** represents the image of experimental setup of XPS spectroscopy.

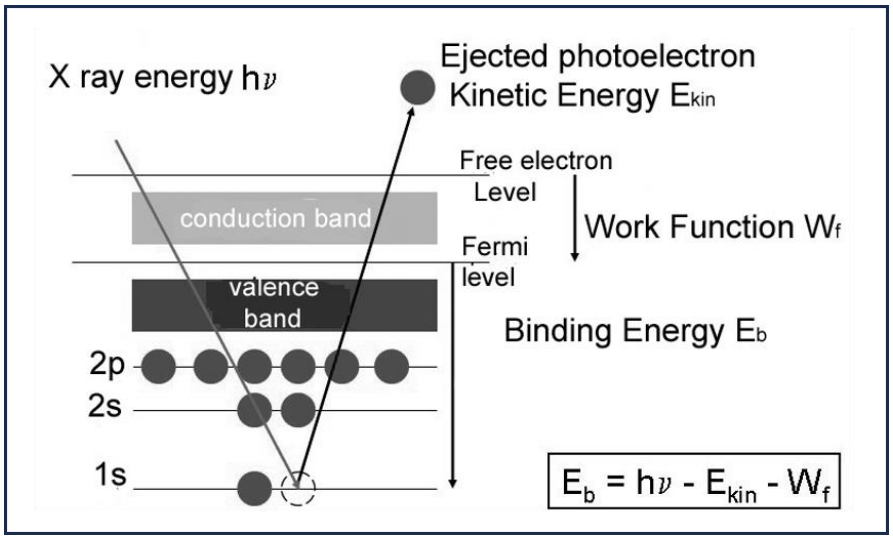

Figure 2.9 Diagram illustrating the basic principle of XPS [22].

Figure 2.10 Experimental setup of XPS spectroscopy, CIF-IIT (BHU), (Thermo Fisher Scientific's K-Alpha spectrometer).

2.3.6 Inductively coupled plasma mass spectrometry (ICP-MS)

Inductively coupled plasma mass spectrometry (ICP-MS) is a type of mass spectrometry (MS) that can detect metals and some nonmetals at concentrations as low as 1 part in 10^{15} (parts per quadrillion) on noninterfered low-background isotopes. This is accomplished by ionising the sample with ICP, then separating, and quantifying those ions with a mass spectrometer. ICP-MS basically made up of six compartments: the sample introduction system, inductively coupled plasma (ICP), interface, ion optics, mass analyser and detector. **Figure 2.11** illustrates a simple diagram of the instrument. In the sample introduction system, liquid samples are first nebulized to produce a fine aerosol, which is then delivered to the argon plasma. After the sample is atomise and ionised by the high-temperature plasma, the ions are extracted through the interface region and into a collection of electrostatic lenses known as the ion optics. The ion beam is directed and focused into the quadrupole mass analyzer by the ion optics. Ions are separated by the mass analyzer based on their mass-charge ratio (m/z), and the detector measures these ions [23, 24]. In this thesis work, Agilent 7800 ICP-MS mainframe was used

to determine the Li, Cr, Fe, Al, Ni in the layered oxides. The experimental setup of inductively coupled plasma mass spectrometry is shown in the **Figure 2.12**.

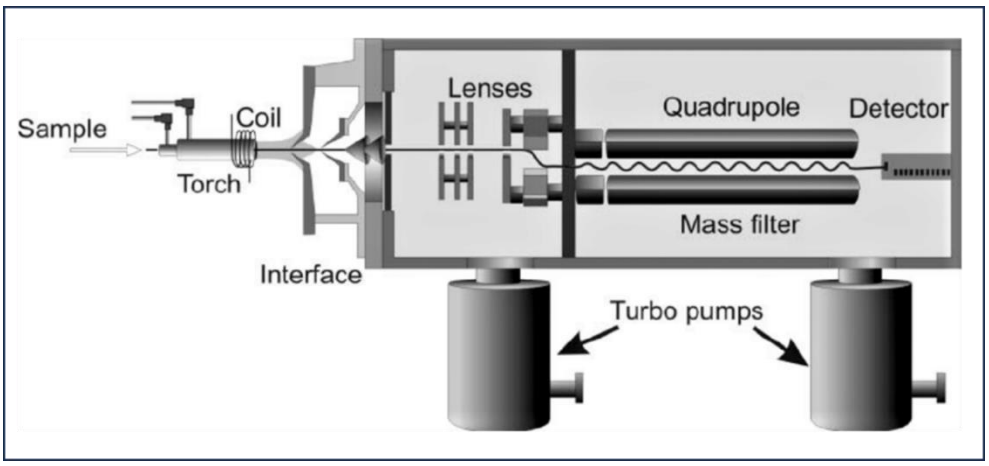

Figure 2.11 Schematic cross section of ICP-MS [23].

Figure 2.12 Experimental setup of ICP-MS, CIF-IIT (BHU), (Agilent 7800 ICP-MS mainframe).

2.3.7 Fourier transform infrared (FTIR) spectroscopy

An essential tool for studying the material's vibrations is infrared spectroscopy. Either by absorbing infrared light or by a molecule's inelastic scattering of the light, it detects molecular vibration. The technique is known as Fourier transform infrared spectroscopy (FTIR) because the computer performs the Fourier transform to turn raw data into an actual spectrum. It takes a short period of time to obtain the spectrum. The obtained spectrum of distinct molecular fingerprints can be further used to screen and scan samples for many different components.

FTIR is usually employed to identify the functional group that's joined to an atom or molecule. An FTIR spectrometer is mainly made up of a light source, monochromatic slit, beam splitter, detector, and an analog recorder [25]. **Figure 2.13** depicts schematic diagram of Fourier transform infrared spectroscope. The FTIR spectra of materials studied in this thesis was measured with Perkin Elmer FTIR spectrometer and data were recorded within 400-4000 cm^{-1} using KBr pellet. **Figure 2.14** displays the image of FTIR measurement CIF-IIT (BHU).

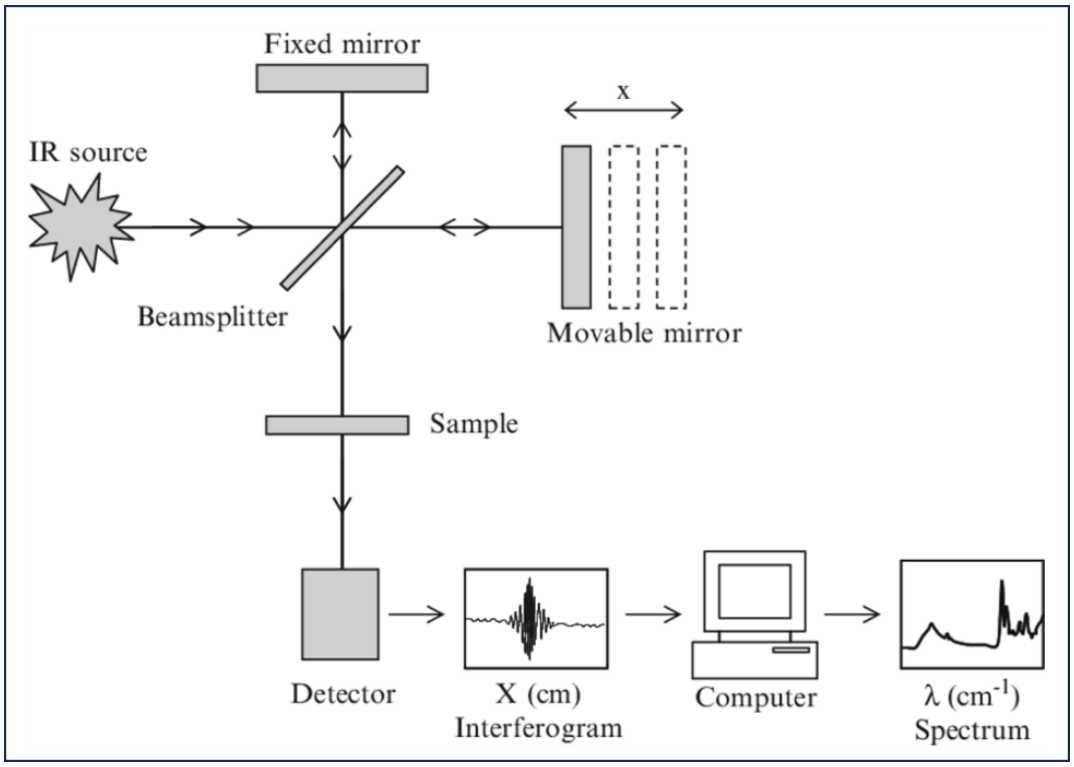

Figure 2.13 Schematic sketch of the essential features of a Fourier transform infrared (FTIR) spectrometer [26].

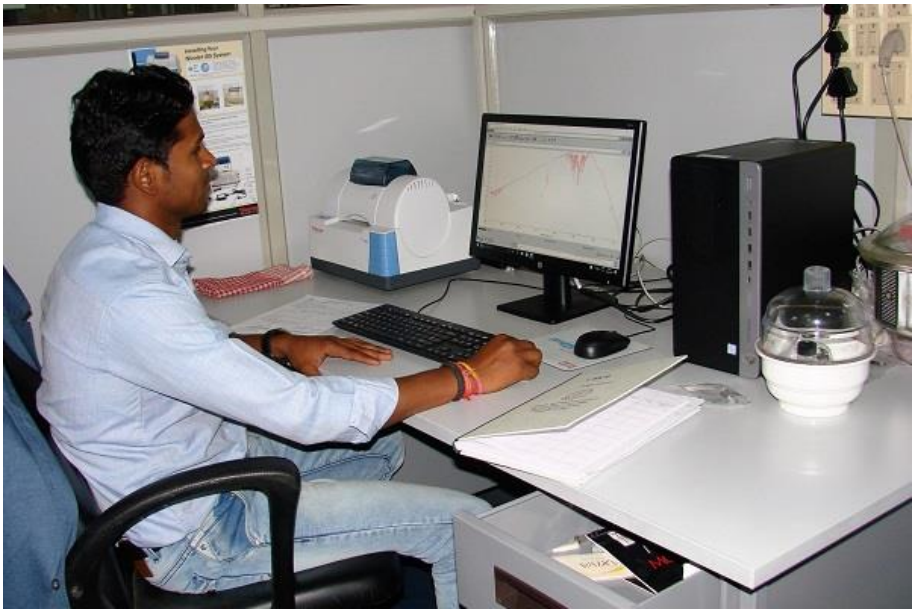

Figure 2.14 Perkin Elmer FTIR spectrometer, CIF-IIT (BHU).

2.3.8 BET (Brunner-Emmett-Teller) surface area measurement

In 1938, Stephen Brunauer, Paul Hugh Emmett, and Edward Teller established the Brunner-Emmett-Teller (BET) theory, which was based on Langmuir's isotherm theory for monolayer molecular adsorption to multilayer adsorption. It attempts to elucidate the physical adsorption of the gas molecule on the solid surface and serving as a useful technique for determining the specific area of materials. Usually, physical adsorption of noncorrosive gas molecules (N_2, Ar, CO_2, etc.) on the surface of material is employed to measure the specific surface area, average pore volume, and pore size distribution of the sample. The hypothesis is predicated on multiple assumptions derived from the Langmuir isotherm theory:

- Adsorption takes place only on well-defined sites of the samples.
- There is no interaction between each adsorption layer.
- Adsorption occurs as a monolayer and each layer is treated as Langmuir monolayer.

Based on the above assumptions, Brunauer, Emmett, and Teller derived the following equation:

$$\frac{1}{\upsilon\left[\left(\frac{p_0}{p}\right)-1\right]} = \frac{c-1}{\upsilon_m}\left(\frac{p_0}{p}\right) + \frac{1}{\upsilon_m} \qquad (2.3)$$

Where υ is the volume of adsorbed gas, υ_m is the volume of adsorbed as monolayer, p_0/p is the relative pressure, c is BET constant, which is defined as

$$c = exp\left(\frac{E_1 - E_L}{RT}\right) \tag{2.4}$$

$$V_{liq} = \frac{P_a + V_{ads} + V_m}{RT} \tag{2.5}$$

E_1 is the adsorption heat for the first layer, and E_L is adsorption heat for the second and higher layers, V_{liq} is the volume of N_2 in the pore, V_{ads} is the volume of gas adsorbed, V_m is the molar volume of liquid adsorbed, P_a is ambient pressure and T is temperature. The plot of $P/\upsilon(P_o-P)$ against P/P_o should provide a straight line because c is a constant for a given gas and is a constant for a given gas-solid system. The slope of the linear plot yields $(c-1)/(\nu_m)$, while the intercept yields $1/(\nu_m)$. Both ν_m and c can be calculated based on the slope and intercept. At different temperatures, a wide number of gas adsorption isotherms on various adsorbents are determined [27, 28]. In the present work, MicrotracBEL BET instrument operated under an N_2 adsorption−desorption medium at 77.3 K were used to analyze the specific surface of the sample. **Figure 2.15** represents the image of experimental setup for the BET analyzer.

Figure 2.15 BET surface area measurement setup, CIF-IIT (BHU), (MicrotracBEL BET instrument).

2.4 Electrochemical characterization

2.4.1 Catalyst ink preparation and electrode fabrication

The catalyst ink was prepared by dispersing 20 mg of catalyst material and 5 mg of activated carbon in 1 ml of N-methyl pyrrolidone (NMP) solvent. Further, 5 µl of Nafion binder was added to the mixture and then ultrasonicated for 30 min to form a homogeneous mixture. The prepared catalyst ink was coated on carbon paper (1 × 1 cm^2) with a loading amount of approximately 1 mg on the carbon substrate. The prepared electrode was then dried at 80 °C for 12 h in a vacuum oven and used as the working electrode. **Figure 2.16a** depicts the procedure of preparing catalysts ink, and **Figure 2.16b** depicts the assembled electrode picture for electrochemical measurement.

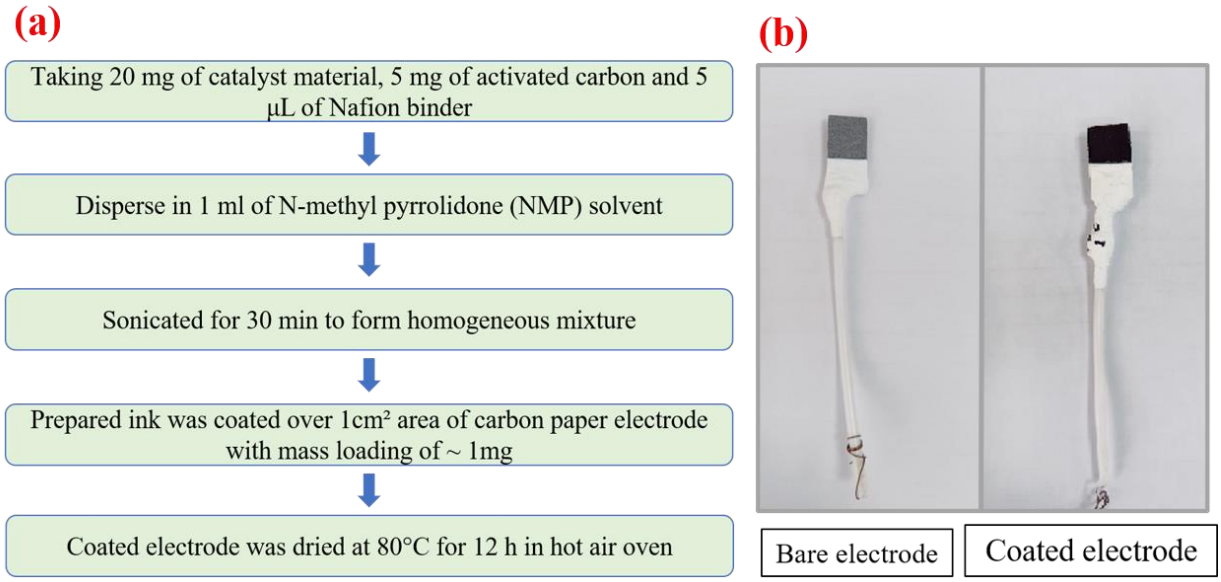

Figure 2.16 (a) Catalyst ink preparation method and **(b)** Assembled electrode picture for electrochemical measurement.

2.4.2 Electrochemical setup

OER measurements were performed by using electrochemical workstation based on Pine research instrument (Wave driver 200) in a conventional three-electrode setup which consists

of catalyst-coated carbon paper of 1 cm^2 area as a working electrode, Ag/AgCl/4M KCl as a reference electrode, and a platinum wire as a counter electrode. All the electrochemical analysis was done with the help of Aftermath software by performing cyclic voltammetry (CV), linear sweep voltammetry (LSV), and electrochemical impedance spectroscopy (EIS) in O_2-saturated 1 M KOH electrolyte. The electrolyte solutions were freshly prepared before each set of experiments from analytical grade KOH (Merck, 85%) and deionized water. All potentials are reported versus the reversible hydrogen electrode (RHE), and for the conversion of the obtained potential (vs Ag/AgCl) to the RHE, the following equation was used.

$$E_{RHE} = E_{Ag/AgCl} + E^0_{Ag/AgCl} + 0.059\,pH \quad (2.6)$$

Where, $E^0_{Ag/AgCl}$ (in 4 M KCl) = + 0.199V; pH = 13.8 for 1 M KOH.

2.4.3 Electrochemical characterization techniques

2.4.3.1 Cyclic voltammetry (CV)

Cyclic Voltammetry (CV) is an electrochemical technique which measures the current that develops in an electrochemical cell under conditions where voltage is in excess of that predicted by the Nernst equation. Like other types of voltammetry, cyclic voltammetry uses a three-electrode system consisting of a working electrode, a reference electrode, and a counter electrode. CV is performed by cycling the potential of a working electrode, and measuring the resulting current. Cyclic voltammetry (CV) is commonly used to investigate the reduction and oxidation processes of molecular species, which is also very helpful to study electron transfer-initiated chemical reactions, including catalysis [29].

In the present study, before collecting the electrochemical data, the working electrode was activated by performing several scans of CV at a scan rate of 100 mV s^{-1} in the range of 0–0.8 V vs. Ag/AgCl. Cyclic voltammetry is also used to perform the durability test and measure the

electrochemical double layer capacitance (C_{dl}) of synthesized catalyst for electrocatalytic OER measurements. Catalyst durability was recorded by using cyclic voltammograms (CVs) at a scan rate of 50 mV s^{-1} for 1000 cycles. The electrochemical double layer capacitance (Cdl) was measured by performing CV at different scan rates of 50, 70, 100, 120, 140 and 160 mV s^{-1} under the potential range of 0.9–0.1 V vs. RHE, where no faradaic current was observed. Current density differences (ΔJ/2) plotted versus scan rates where the slope represents Cdl.

2.4.3.2 Linear sweep voltammetry (LSV)

Linear sweep voltammetry (LSV) is a simple electrochemical method that only requires a single linear sweep from the lower potential limit to the upper potential limit. This is especially helpful for systems that are irreversible, meaning that a reverse sweep would not yield any further information. Like cyclic voltammetry, LSV uses a three-electrode setup consisting of a working electrode, counter electrode, and reference electrode. It measures the current flowing through a working electrode while the potential between the working electrode and a reference electrode is linearly sweeping over time. The peak current, peak current potential, and half-peak current potential can all be determined using linear sweep voltammetry. Linear sweep voltammetry is a quick and easy substitute for cyclic voltammetry in irreversible systems [30]. In the present work, linear sweep voltammograms (LSVs) were performed at a scan rate of 5 mV s^{-1} from 0 to 0.8 V vs. Ag/AgCl. LSV curves is used to measure the overpotential and Tafel slope value of synthesized catalysts for OER. Tafel slope is calculated by plotting overpotential (η) versus the logarithm of current density (log |j|), which could investigate the kinetics of the OER catalysts.

2.4.3.3 Electrochemical impedance spectroscopy (EIS)

Impedance is a measure of the ability of a circuit to resist the flow of electrical current. Electrochemical impedance spectroscopy (EIS) uses the application of a small sinusoidal

potential to the working electrode in an electrochemical cell, while measuring the resulting current response. By varying the excitation frequency, f, of the applied potential over a range of frequencies, one can calculate the complex impedance; the sum of the real and imaginary impedance components of the system as a function of the frequency (i.e., angular frequency w). Therefore, EIS combines the analysis of both real and imaginary components of impedance, namely, the electrical resistance and reactance [31]. In the present work, electrochemical impedance spectroscopy (EIS) was performed to investigate the charge-transfer kinetics at the electrode/electrolyte interface, which was conducted with AC voltage with 10 mV amplitude at certain potential within the frequency range from 0.1 Hz to 100 kHz.

2.4.3.4 Chronoamperometry (CA)

Chronoamperometry is a time-dependent technique where a square-wave potential is applied to the working electrode. The current of the electrode, measured as a function of time, fluctuates according to the diffusion of an analyte from the bulk solution toward the sensor surface [31]. Long term stability test of materials synthesized in this thesis work was measured by chronoamperometric measurements which is conducted at a constant potential to maintain an initial current density of 10 mA cm^{-2} over 12 h.

2.5 References

1. Jansen, M., 2002. A concept for synthesis planning in solid-state chemistry. *Angewandte Chemie International Edition*, *41*(20), pp.3746-3766.
2. Smida, Y.B., Marzouki, R., Kaya, S., Erkan, S., Zid, M.F. and Hamzaoui, A.H., 2020. Synthesis Methods in Solid-State Chemistry. *Synthesis Methods and Crystallization, Intech Open.* doi: 10.5772/intechopen.93337.
3. Evecan, D., Kaplan, Ş.S., Sönmez, M.Ş., Yıldırım, S., Okutan, M., Deligöz, H. and Zayim, E., 2019. Smart glass electrochromic device fabrication of uniform tungsten oxide films from its powder synthesized by solution combustion method. *Microelectronic Engineering*, *215*, p.110989.
4. González-Cortés, S.L. and Imbert, F.E., 2013. Fundamentals, properties and applications of solid catalysts prepared by solution combustion synthesis (SCS). *Applied Catalysis A: General*, *452*, pp.117-131.
5. Banger, K.K., Yamashita, Y., Mori, K., Peterson, R.L., Leedham, T., Rickard, J. and Sirringhaus, H.J.N.M., 2011. Low-temperature, high-performance solution-processed metal oxide thin-film transistors formed by a 'sol–gel on chip'process. *Nature Materials*, *10*(1), pp.45-50.
6. Shao, Z., Zhou, W. and Zhu, Z., 2012. Advanced synthesis of materials for intermediate-temperature solid oxide fuel cells. *Progress in Materials Science*, *57*(4), pp.804-874.
7. Danks, A.E., Hall, S.R. and Schnepp, Z.J.M.H., 2016. The evolution of 'sol–gel'chemistry as a technique for materials synthesis. *Materials Horizons*, *3*(2), pp.91-112.
8. Birol, H., Rambo, C.R., Guiotoku, M. and Hotza, D., 2013. Preparation of ceramic nanoparticles via cellulose-assisted glycine nitrate process: a review. *Rsc Advances*, *3*(9), pp.2873-2884.
9. Patil, K.C., 2008. *Chemistry of nanocrystalline oxide materials: combustion synthesis, properties and applications*. World Scientific.
10. Drits, V., Środoń, J. and Eberl, D.D., 1997. XRD measurement of mean crystallite thickness of illite and illite/smectite: Reappraisal of the Kubler index and the Scherrer equation. *Clays and Clay Minerals*, *45*, pp.461-475.
11. Thodeti, S., Reddy, R.M. and Kumar, J.S., 2016. Synthesis and characterization of pure and indium doped SnO_2 nanoparticles by sol-gel methods. *Int. J. Sci. Eng. Res*, *7*, pp.310-317.
12. Guo, J., Meng, Z., Qiao, Y. and Li, B., 2023, February. Numerical Analysis of Structural Color for Photonic Crystal Hydrogel. In *Photonics* (Vol. 10, No. 2, p. 186). MDPI.

13. Ho, K.M., Chan, C.T. and Soukoulis, C.M., 1990. Existence of a photonic gap in periodic dielectric structures. *Physical Review Letters*, *65*(25), p.3152.
14. Rietveld, H.M., 1969. A profile refinement method for nuclear and magnetic structures. *Journal of applied Crystallography*, *2*(2), pp.65-71.
15. Chaudhari, S., 1999, December. Electron microscopy: an essential tool for the synthesis of thin film for practical applications. In *Proceeding of national conference on electron microscopy at DMSRDE* (pp. 1-3).
16. Pennycook, S.J. and Nellist, P.D. eds., 2011. *Scanning transmission electron microscopy: imaging and analysis*. Springer Science & Business Media.
17. Inkson, B.J., 2016. Scanning electron microscopy (SEM) and transmission electron microscopy (TEM) for materials characterization. In *Materials characterization using nondestructive evaluation (NDE) methods* (pp. 17-43). Woodhead publishing.
18. Scimeca, M., Bischetti, S., Lamsira, H.K., Bonfiglio, R. and Bonanno, E., 2018. Energy Dispersive X-ray (EDX) microanalysis: A powerful tool in biomedical research and diagnosis. *European journal of histochemistry: EJH*, *62*(1).
19. Carter, C.B. and Williams, D.B. eds., 2016. *Transmission electron microscopy: Diffraction, imaging, and spectrometry*. Springer.
20. Kohl, H. and Reimer, L., 2008. Transmission Electron Microscopy. *Springer Series in Optical Sciences*, *36*.
21. Van der Heide, P., 2011. *X-ray photoelectron spectroscopy: an introduction to principles and practices*. John Wiley & Sons.
22. Mane, A.T. and Patil, V.B., 2016. X-ray photoelectron spectroscopy of nanofillers and their polymer nanocomposites. In *Spectroscopy of Polymer Nanocomposites* (pp. 452-467). William Andrew Publishing.
23. Nageswaran, G., Choudhary, Y.S. and Jagannathan, S., 2017. Inductively coupled plasma mass spectrometry. In *Spectroscopic methods for nanomaterials characterization* (pp. 163-194). Elsevier.
24. Košler, J. and Sylvester, P.J., 2003. Present trends and the future of zircon in geochronology: laser ablation ICPMS. Reviews inMineralogy and Geochemistry 53 (1), 243–275.
25. De Haseth, J.A., 1982. Fourier transform infrared spectrometry. In *Fourier, Hadamard, and Hilbert Transforms in Chemistry* (pp. 387-420). Boston, MA: Springer US.

26. Ojeda, J.J. and Dittrich, M., 2012. Fourier transform infrared spectroscopy for molecular analysis of microbial cells. *Microbial Systems Biology: Methods and Protocols*, pp.187-211.
27. Naderi, M., 2015. Surface area: brunauer–emmett–teller (BET). In *Progress in filtration and separation* (pp. 585-608). Academic Press.
28. Bardestani, R., Patience, G.S. and Kaliaguine, S., 2019. Experimental methods in chemical engineering: specific surface area and pore size distribution measurements—BET, BJH, and DFT. *The Canadian Journal of Chemical Engineering*, *97*(11), pp.2781-2791.
29. Elgrishi, N., Rountree, K.J., McCarthy, B.D., Rountree, E.S., Eisenhart, T.T. and Dempsey, J.L., 2018. A practical beginner's guide to cyclic voltammetry. *Journal of chemical education*, *95*(2), pp.197-206.
30. Bard, A.J., Faulkner, L.R. and White, H.S., 2022. *Electrochemical methods: fundamentals and applications*. John Wiley & Sons.
31. Guy, O.J. and Walker, K.A.D., 2016. Graphene functionalization for biosensor applications. *Silicon Carbide Biotechnology*, pp.85-141.